White Rose Research Online

eprints@whiterose.ac.uk
https://eprints.whiterose.ac.uk
Universities of Leeds, Sheffield and York

Deposited via The University of Sheffield.

White Rose Research Online URL for this paper:
https://eprints.whiterose.ac.uk/id/eprint/246507/

Version: Accepted Version

Proceedings Paper:
Yu, H., Saad, R. and Ball, E.A. (2026) Thinned coding patterns for reflection magnitude control in a multi-functional reconfigurable reflective surface. In: 2026 19th United Conference on Millimeter Waves and Terahertz Technologies (UCMMT). 2026 19th United Conference on Millimeter Waves and Terahertz Technologies (UCMMT), 23-26 Aug 2026, Birmingham, United Kingdom. Institute of Electrical and Electronics Engineers (IEEE), pp. 1-4. ISBN: 9798319536570. ISSN: 2639-4545. EISSN: 2639-4537.

https://doi.org/10.1109/ucmmt70119.2026.11719270

© 2026 The Authors. Except as otherwise noted, this author-accepted version of a conference paper published in 2026 19th United Conference on Millimeter Waves and Terahertz Technologies (UCMMT) is made available via the University of Sheffield Research Publications and Copyright Policy under the terms of the Creative Commons Attribution 4.0 International License (CC-BY 4.0), which permits unrestricted use, distribution and reproduction in any medium, provided the original work is properly cited. To view a copy of this licence, visit http://creativecommons.org/licenses/by/4.0/

Reuse
This article is distributed under the terms of the Creative Commons Attribution (CC BY) licence. This licence allows you to distribute, remix, tweak, and build upon the work, even commercially, as long as you credit the authors for the original work. More information and the full terms of the licence here: https://creativecommons.org/licenses/

Takedown
If you consider content in White Rose Research Online to be in breach of UK law, please notify us by emailing eprints@whiterose.ac.uk including the URL of the record and the reason for the withdrawal request.

UNIVERSITY OF LEEDS
University of Sheffield
UNIVERSITY of York

Thinned Coding Patterns for Reflection Magnitude Control in a Multi-Functional Reconfigurable Reflective Surface

Hang Yu
School of Electrical and Electronic Engineering
University of Sheffield
Sheffield, U.K.
hyu37@sheffield.ac.uk

Rola Saad
Department of Medical Physics and Biomedical Engineering
University College London
London, U.K.
r.saad@ucl.ac.uk

Edward A. Ball
School of Electrical and Electronic Engineering
University of Sheffield
Sheffield, U.K.
e.a.ball@sheffield.ac.uk

***Abstract*—Reconfigurable intelligent surfaces are distinguished by their ability to enable controlled propagation environments and support multi-functional electromagnetic responses. However, increasing hardware complexity and power consumption remain key challenges for practical, large-scale implementations. This paper investigates spatial-domain magnitude control on an 8×8 reconfigurable reflective surface through geometric coding patterns, with analysis conducted at 5.05 GHz and 5.50 GHz. The relationship between reflection magnitude, active element density and spatial distribution is examined across 34 coding patterns. Results show that reflection magnitudes of -6 dB and -10 dB can each be achieved with as few as 12 active elements (19% of the surface) at 5.05 GHz, and that reflection magnitude at 5.50 GHz exhibits a consistent dependence on active element density. In addition, a first-order analytical approximation is introduced to estimate the reflection magnitude of selected patterns, providing reasonable agreement for most cases and capturing the underlying trend for ring-based configurations. The findings demonstrate the feasibility of a thinned coding pattern for multi-functional RIS, with potential for reduced hardware overhead and improved power efficiency at scale.**

***Index Terms*—RIS, magnitude control, thinned coding pattern, RF hardware**

I. Introduction

Future wireless networks are expected to deliver precise localization, advanced sensing, high energy efficiency, and seamless integration with intelligent systems. Reconfigurable intelligent surfaces (RIS), also referred to as programmable metasurfaces, represent one promising solution to fulfil these requirements [1]. By enabling programmable manipulation of the propagation environment, RIS allows dynamic shaping of the wireless channel. This capability underpins the concept of the smart radio environment [2], where communication performance is enhanced through deliberate electromagnetic (EM) control.

Extensive research has focused on improving the multifunctionality and EM control capabilities of RIS [3], [4], [5]. While most work has emphasized multi-bit phase control, magnitude control has been explored as a complementary capability, often combined with phase tuning, to expand the achievable EM response and enable a broader range of functionalities. Precise control of reflection magnitude supports applications including radar cross-section (RCS) control, interference mitigation in multi-user scenarios [6], [7], and communication-oriented functions such as multi-level amplitude shift keying (ASK). The latter enables higher-order modulation without requiring complex RF modulation chains [8], allowing RIS to move beyond passive wave redirection toward a more integrated role within the communication system [9].

However, realizing these capabilities introduces significant hardware challenges. Multi-level quantization and multifunctionality typically require integrating additional tunable components, such as PIN diodes, varactors or RF-switch within each unit cell [5], [10]. This directly increases control complexity and overall power consumption [11]. The challenge becomes more critical at higher frequencies, where smaller unit cell dimensions require more elements to cover the same physical area. The result is greater control complexity and increasingly difficult power management at the system level.

In our previous work [12], we proposed a low-power, dual-mode reconfigurable reflective surface based on the single-pole double-throw (SPDT) RF switch, in which ring-based geometric pattern configurations further enabled magnitude control through spatial coding, with initial results showing that edge-located unit cells play a dominant role in magnitude control at 5.05 GHz. Moreover, activating only 48 of the 64 unit cells (75%) achieved absorptive performance within 0.5 dB of full-surface operation at 5.50 GHz, providing initial evidence that a thinned coding pattern, in which only a subset of unit cells requires active switching, may be sufficient to maintain the desired surface functionality. However, the influence of active element density and spatial distribution on the reflection response was not systematically investigated.

This paper therefore extends the prior work by evaluating all 34 available coding patterns, comprising 10 ring-based configurations from [12] and 24 additional patterns, and analysing their impact on reflection magnitude at 5.05 GHz and 5.50

This work was supported in part by U.K. Engineering and Physical Sciences Research Council (EPSRC) through the Doctoral Training Partnership (DTP) under Grant EP/W524360/1 and in part by U.K. Research and Innovation (UKRI) Future Leaders Fellowship under Grant UKRI1064.

GHz. The aim is to clarify the roles of active element density and spatial distribution in magnitude control, and to provide further insight into scalable, low-power RIS implementations.

II. Impact of Pattern Geometry and Spatial Arrangement

A. Full Surface Configuration and Performance

As a baseline, two full-surface configurations are defined, in which all 64 unit cells are uniformly set to either State '0' or State '1', represented by white and green respectively in Fig. 1. These states correspond to the low and high control voltage levels applied to the RF switches respectively.

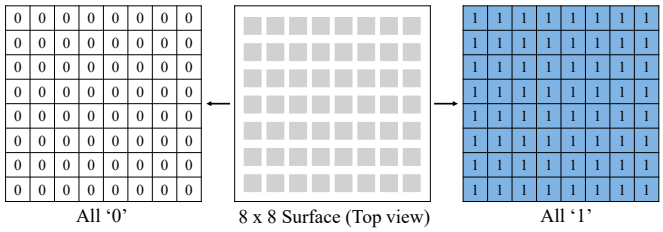


Fig. 1. The 8 × 8 surface under the all-'0' configuration (left) and the all-'1' configuration (right), represented by blank and green unit cells, respectively.

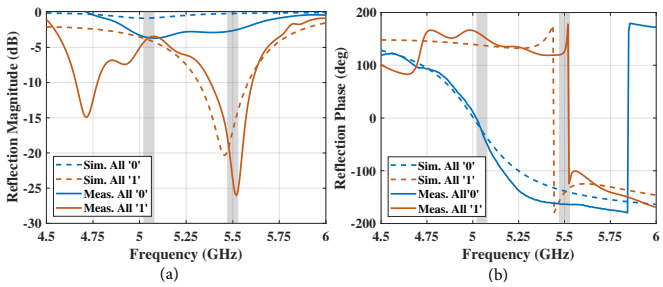


Fig. 2. Measured reflection (a) magnitude and (b) phase under the all-'0' and all-'1' configurations, as defined in Fig. 1. Results are reproduced from [12]. Grey shading indicates the frequencies of interest at 5.05 GHz and 5.50 GHz.

The measured reflection responses for both configurations are reproduced from [12] and presented in Fig. 2, with two frequency regions of interest highlighted in grey at 5.05 GHz and 5.50 GHz. At 5.05 GHz, switching between the two states results in approximately 180° phase shift while the reflection magnitude remains nearly constant. At 5.50 GHz, the surface transitions from a reflective to an absorptive state when the switch state changes from all-'0' to all-'1'. These baseline responses serve as the reference against which all coding patterns in this study are evaluated. For clarity, the surface operating states at 5.05 GHz and 5.50 GHz are hereafter referred to as the *'phase mode'* and *'magnitude mode'*, respectively, based on their dominant switching response shown in Fig. 2.

B. Impact of Active Element Density

The measured reflection coefficient of each coding pattern was classified by the number of active ('1') elements. The corresponding reflection magnitude in the phase and magnitude mode, as a function of active element density, is presented in Fig. 3. In the phase mode, no consistent correlation is observed between active element density and reflection magnitude, as shown in Fig. 3(a). Comparable reflection levels can be achieved with significantly fewer active unit cells. Two representative cases are shown in Fig. 4, where patterns with different densities achieve approximately -6 dB and -10 dB, each with magnitude deviations within ±0.5 dB. This indicates that the desired reflection magnitude can be achieved without activating the maximum number of elements, directly reducing control complexity and improving energy efficiency at the system level.

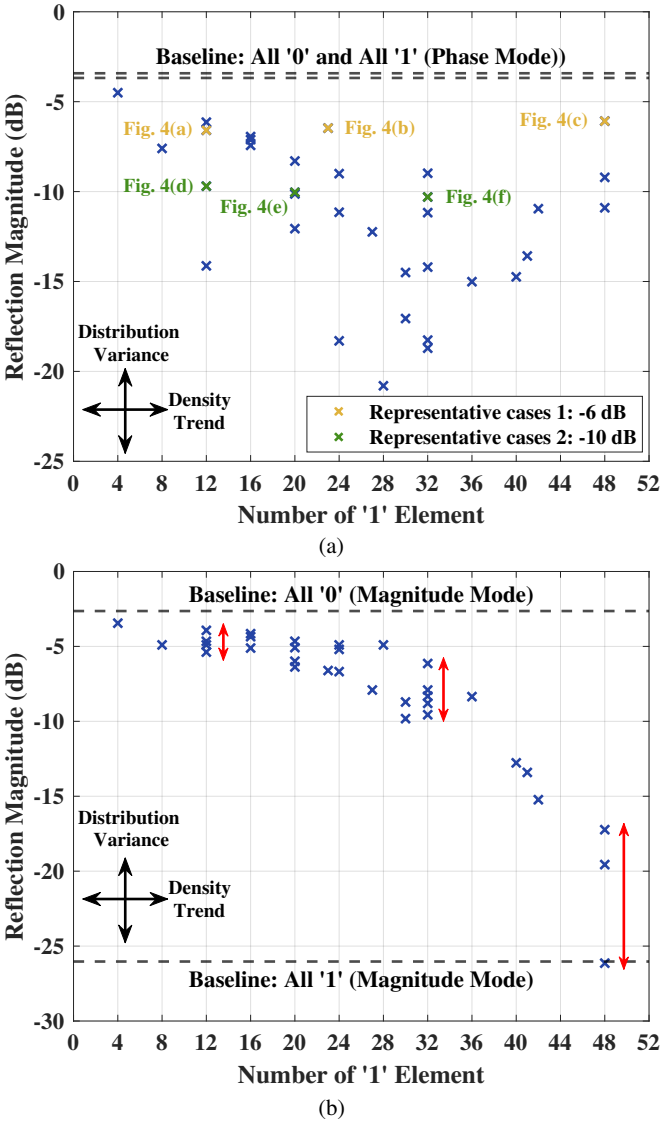


Fig. 3. Reflection magnitude as a function of element density, based on 34 measured geometric coding patterns: (a) phase mode and (b) magnitude mode. Dotted lines indicate the baseline reflection magnitudes corresponding to the all-'0' and all-'1' full-surface configurations, as defined in Fig. 2.

In contrast, the reflection magnitude response in the magnitude mode shows a more consistent dependence on active element density. As shown in Fig. 3(b), the reflection magnitude remains relatively stable, varying by no more than 2 dB,

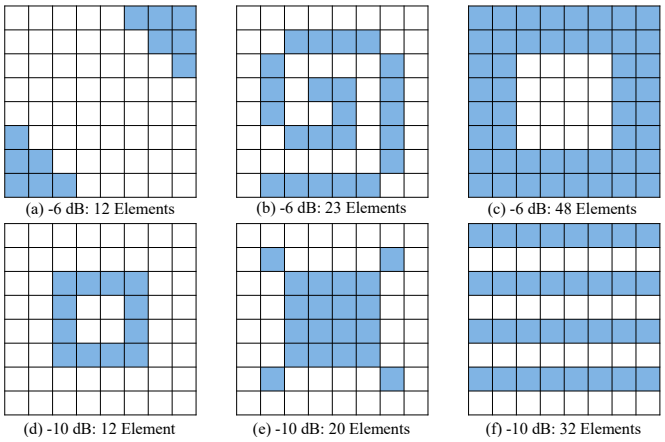


Fig. 4. Representative coding patterns in the phase mode achieving reflection magnitudes of -6 dB and -10 dB with varying active element densities. Case 1 (approximately -6 dB): (a) 12, (b) 23, and (c) 48 active ('1') elements. Case 2 (approximately -10 dB): (d) 12, (e) 20, and (f) 32 active ('1') elements.

for patterns containing up to 24 active elements (38% density). A pronounced roll-off is observed for patterns containing 32 or more active elements ($\geq$50% density), relative to the full dynamic range defined by the all-'0' and all-'1' configurations.

This difference in density dependence between the two modes is attributed to the 180° phase shift available in the phase mode, which is absent in the magnitude mode where the reflected phase remains negligible under low reflection magnitude conditions.

C. Spatial Distribution of Active Elements

To further examine the influence of spatial distribution, the density plots were analysed at fixed active element counts. For patterns with the same number of active ('1') elements, variations in reflection magnitude are attributed to differences in spatial arrangement rather than element density alone. In the phase mode, patterns with identical densities show substantial variation in reflection magnitude, up to 10 dB at a count of 32 active elements, indicating that spatial arrangement plays a dominant role in this mode. This behaviour is consistent with phase interactions between unit cells, where the relative positions of active elements govern the degree of phase superposition or cancellation across the surface.

In contrast, in the magnitude mode, patterns with the same active element count show smaller deviations in reflection magnitude, indicated by the red arrows in Fig. 3(b). The response at this frequency follows a more additive behaviour, in which the overall reflection magnitude decreases progressively with increasing active element count. This suggests that, in the magnitude mode, element density is the primary factor governing magnitude control, with spatial arrangement playing a secondary role.

III. Analytical Approximation of Reflection Magnitude in the Phase Mode

To approximate the reflection magnitude of the applied coding patterns in the phase mode, a first-order spatial summation model is used, incorporating free-space path loss and spatial phase delay. The model is based on the measurement geometry illustrated in Fig. 5, with both the transmitting and receiving horns positioned at normal incidence to the surface.

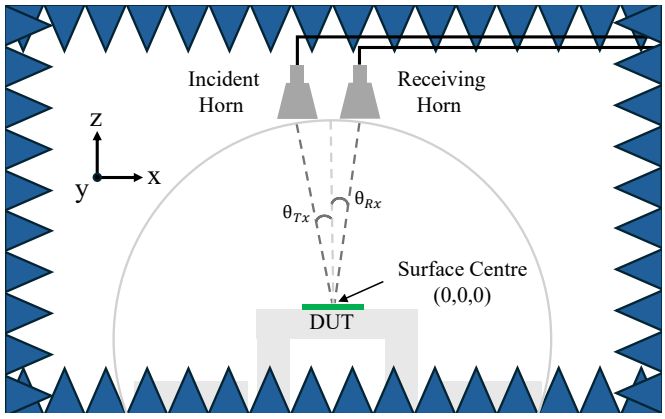


Fig. 5. Geometry of the measurement in the xz-plane for analytical approximation, based on the NRL arch anechoic chamber setup.

Under this configuration, the total received field E_{rx} at the receiving horn is expressed as:

$$E_{rx} = \sum_{n=1}^{64} \Gamma_n \left(\frac{1}{d_{Tx,n} \cdot d_{Rx,n}} \right) e^{-jk(d_{Tx,n}+d_{Rx,n})} \quad (1)$$

where Γ_n denotes the complex reflection coefficient of the n^{th} unit cell, $d_{Tx,n}$ and $d_{Rx,n}$ are the effective path lengths from the transmitting and receiving horns to the n^{th} unit cell, as defined in Fig. 5. k denotes the free-space wavenumber.

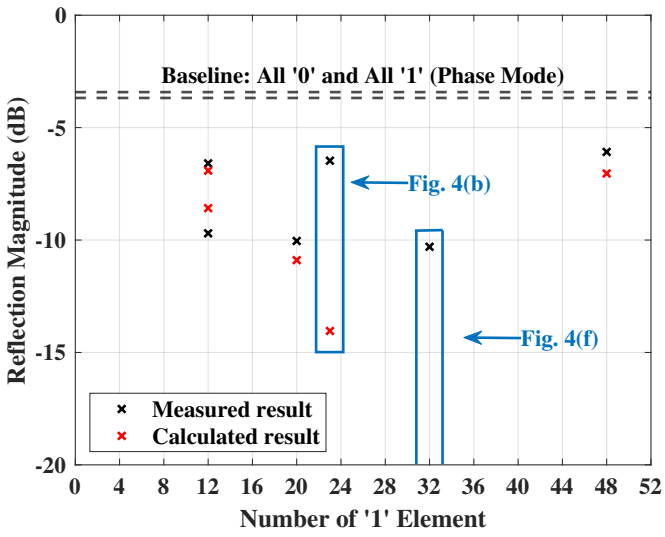


Fig. 6. Measured and calculated reflection magnitudes in the phase mode for the coding patterns shown in Fig. 4, using the analytical approximation in (1). Two patterns with large prediction errors are highlighted by blue boxes.

A comparison between the measured and calculated reflection magnitudes from (1) for the two representative cases in Fig. 4 is presented in Fig. 6. For most patterns, the calculated

values agree with measurements to within 1.2 dB. However, the patterns in Fig. 4(b) and Fig. 4(f) exhibit larger deviations. In particular, the pattern in Fig. 4(f) yields a predicted near-total cancellation, whereas the measured value is -10 dB. This deviation is attributable to several practical factors. In the physical setup, imperfect horn alignment introduces additional phase offsets that are not fully captured by the model, partially mitigating the predicted cancellation. Furthermore, discrepancies arise from unmodelled physical effects, primarily mutual coupling between adjacent unit cells and edge diffraction caused by the finite surface aperture.

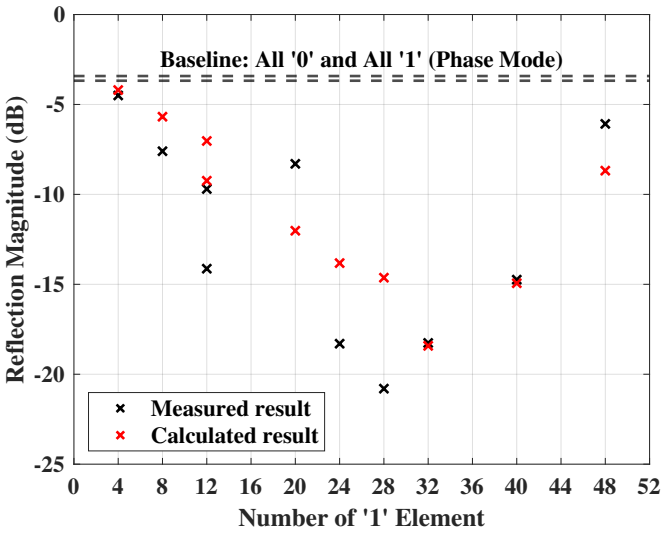


Fig. 7. Measured and calculated reflection magnitudes in the phase mode for the ten ring-based coding patterns defined in [12], using the analytical approximation in (1).

To assess the model over a more structured set of configurations, the approximation was applied to the ring-based coding patterns from [12]. The measured and calculated results are presented in Fig. 7, deviations between the two are likely attributable to the same unmodelled effects noted above, compounded by the clustered spatial arrangement of active elements in certain ring configurations. Nevertheless, the model captures the underlying trend across the ring-based pattern sets, providing useful first-order insight into how the reflection magnitude varies with spatial configuration.

IV. Conclusion

In this work, the reflection behaviour of an 8×8 reconfigurable reflective surface under 34 geometric coding patterns has been investigated. Reflection magnitude was analysed in the phase mode (5.05 GHz) and in the magnitude mode (5.50 GHz) with respect to active element density and spatial distribution. The results demonstrate that a thinned coding patterns can be implemented in a multi-functional RIS with magnitude control capability. Specifically, certain patterns achieve a controlled reflection magnitude with as few as 12 active elements (19% of the total surface), directly reducing control complexity and power consumption at the system level.

In addition, a first-order analytical approximation for reflection magnitude was developed and validated for a defined set of coding patterns. The model shows reasonable agreement with measured results for certain patterns, with deviations likely attributable to mutual coupling between neighbouring unit cells or element clusters and the edge diffraction effect. For the structured ring-based patterns, the approximation provides a useful first-order estimate of the reflection trend, despite the prediction errors introduced by the model's simplifying assumptions.

References

[1] M. Di Renzo, K. Ntontin, J. Song, F. H. Danufane, X. Qian, F. Lazarakis, J. De Rosny, D.-T. Phan-Huy, O. Simeone, R. Zhang, M. Debbah, G. Lerosey, M. Fink, S. Tretyakov, and S. Shamai, "Reconfigurable Intelligent Surfaces vs. Relaying: Differences, Similarities, and Performance Comparison," *IEEE Open J. Commun. Soc.*, vol. 1, pp. 798–807, 2020.

[2] M. Di Renzo, A. Zappone, M. Debbah, M.-S. Alouini, C. Yuen, J. de Rosny, and S. Tretyakov, "Smart Radio Environments Empowered by Reconfigurable Intelligent Surfaces: How It Works, State of Research, and The Road Ahead," *IEEE J. Sel. Areas Commun.*, vol. 38, no. 11, pp. 2450–2525, Nov. 2020.

[3] J. Y. Dai, J. Zhao, Q. Cheng, and T. J. Cui, "Independent control of harmonic amplitudes and phases via a time-domain digital coding metasurface," *Light Sci. Appl.*, vol. 7, no. 1, p. 90, Nov. 2018.

[4] W. Li, H. Guo, X. Wang, G.-M. Yang, and Y.-Q. Jin, "A 2-bit Reconfigurable Metasurface With Real-Time Control for Deflection, Diffusion, and Polarization," *IEEE Trans. Antennas Propag.*, vol. 72, no. 2, pp. 1521–1531, Feb. 2024.

[5] N. Yang, Y. C. Zhong, Y. Wang, Y. Jia, J.-Q. Zhu, Z.-X. Liu, and Y. Liu, "A 2-Bit Programmable Reflectarray Antenna Based on a Polarization-Insensitive Metasurface," *IEEE Trans. Antennas Propag.*, vol. 72, no. 7, pp. 5539–5549, Jul. 2024.

[6] Y. H. Liu, S. Y. Wang, K. N. Qi, and Y. B. Li, "Dynamic Controlling the Bistatic RCS by Programmable Metasurface With Continuous and Independent Manipulation of Reflective Phase and Amplitude," *IEEE Antennas Wirel. Propag. Lett.*, vol. 23, no. 3, pp. 1000–1004, Mar. 2024.

[7] F. Wang and A. L. Swindlehurst, "Applications of Absorptive Reconfigurable Intelligent Surfaces in Interference Mitigation and Physical Layer Security," *IEEE Trans. Wirel. Commun.*, vol. 23, no. 5, pp. 3918–3931, May 2024.

[8] J. Y. Dai, W. Tang, L. X. Yang, X. Li, M. Z. Chen, J. C. Ke, Q. Cheng, S. Jin, and T. J. Cui, "Realization of Multi-Modulation Schemes for Wireless Communication by Time-Domain Digital Coding Metasurface," *IEEE Trans. Antennas Propag.*, vol. 68, no. 3, pp. 1618–1627, Mar. 2020.

[9] T. J. Cui, L. Li, S. Liu, Q. Ma, L. Zhang, X. Wan, W. X. Jiang, and Q. Cheng, "Information Metamaterial Systems," *iScience*, vol. 23, no. 8, p. 101403, Aug. 2020.

[10] J. Zhao, S. Qiao, H. Topozlu, J. Wu, M. M. Honari, J. H. Booske, and N. Behdad, "Electronically Reconfigurable Reflectarray Antennas Using 2-bit Phase Shift Unit Cells Embedded With Reflecting Circuits," *IEEE Trans. Antennas Propag.*, vol. 73, no. 1, pp. 314–328, Jan. 2025.

[11] J. Wang, W. Tang, J. C. Liang, L. Zhang, J. Y. Dai, X. Li, S. Jin, Q. Cheng, and T. J. Cui, "Reconfigurable Intelligent Surface: Power Consumption Modeling and Practical Measurement Validation," *IEEE Trans. Commun.*, pp. 1–1, 2024.

[12] H. Yu, E. A. Ball, and R. Saad, "An RF-Switch-Enabled Low-Power Dual-Mode Reconfigurable Reflective Surface," *IEEE Open J. Antennas Propag.*, pp. 1–1, 2026.